Assessment of CAR-T Cell-Mediated Cytotoxicity in 3D Microfluidic Cancer Co-Culture Models for Combination Therapy

Karla Paterson, Sarah Paterson, Theresa Mulholland, Seth B. Coffelt, and Michele Zagnoni

***Abstract*—Chimeric antigen receptor (CAR)-T cell therapy is efficacious against many haematological malignancies, but challenges remain when using this cellular immunotherapy for treating solid tumours. Classical 2D *in vitro* models fail to recapitulate the complexity of the tumour microenvironment, whilst *in vivo* models, such as patient-derived xenografts, are costly and labour intensive. Microfluidic technologies can provide miniaturized solutions to assess CAR-T therapies in 3D complex preclinical models of solid tumours. Here, we present a novel microfluidic immunoassay for the evaluation of CAR-T cell cytotoxicity and targeting specificity on 3D spheroids containing cancer cells and stromal cells. Monitoring the interaction between CAR-T cells and spheroid co-cultures, we show that CAR-T cells home towards target-expressing cancer cells and elicit a cytotoxic effect. Testing CAR-T cells in combination therapies, we show that CAR-T cell cytotoxicity is enhanced with anti-PD-L1 therapy and carboplatin chemotherapy. We propose this proof-of-concept microfluidic immunoassay as a material-saving, pre-clinical screening tool for quantification of cell therapy efficacy.**

***Index Terms*—Immunotherapy, lab-on-a-chip, solid tumour microenvironment, three-dimensional in vitro complex model.**

***Impact Statement*—Microfluidic platforms and protocols can provide powerful, cost-effective and miniaturised in vitro assays to preclinically assess CAR-T cell therapies in solid tumours.**

Manuscript received February 4, 2022; revised May 16, 2022 and May 23, 2022; accepted May 23, 2022. Date of publication May 27, 2022; date of current version June 15, 2022. This work was supported in part by AMS Biotechnology Europe Ltd through industrial Ph.D. studentship to Karla Paterson and Michele Zagnoni and in part by internal funds by Strathclyde University to Michele Zagnoni and Karla Paterson. The review of this article was arranged by Associate Editor Ambika Bajpayee. *(Corresponding author: Michele Zagnoni.)*

Karla Paterson and Michele Zagnoni are with the Centre for Microsystems and Photonics, EEE Department, University of Strathclyde, G1 1XQ Glasgow, U.K., and also with the ScreenIn3D Limited, Technology and Innovation Centre, G1 1RD Glasgow, U.K. (e-mail: karla.findlay@strath.ac.uk; michele.zagnoni@strath.ac.uk).

Sarah Paterson and Theresa Mulholland are with the ScreenIn3D Limited, Technology and Innovation Centre, G1 1RD Glasgow, U.K. (e-mail: sarahpaterson1996@gmail.com; theresa.christ@gmail.com).

Seth B. Coffelt is with the Institute of Cancer Sciences, University of Glasgow, Glasgow G12 8QQ, U.K., and also with the Cancer Research U.K. Beatson Institute, Glasgow G61 1BD, U.K. (e-mail: seth.coffelt@glasgow.ac.uk).

This article has supplementary downloadable material available at https://doi.org/10.1109/OJEMB.2022.3178302, provided by the authors.

Digital Object Identifier 10.1109/OJEMB.2022.3178302

I. Introduction

CHIMERIC antigen receptor (CAR)-T cell immunotherapies have been remarkably successful in the treatment of haematological malignancies and focus has now shifted to harnessing this technology towards tackling solid tumours. [1] As examples, the most targeted antigens in CAR-T clinical trials in patients with epithelial malignancies have been epidermal growth factor receptor (EGFR), human epidermal growth factor receptor 2 (HER2) and natural killer group 2D (NKG2D)-ligands.[2] However, there are several reasons impairing widespread application of CAR-T therapy. CAR-T cell production is associated with high manufacturing costs due to the autologous acquisition process from patients[3] and off-target toxicity can trigger serious or even life-threatening therapy response.[1], [4], [5] Specific to solid tumours, CAR-T cell infiltration is hindered by the immunosuppressive tumour microenvironment (TME), this comprising a variety of cell types releasing an assortment of cytokines, chemokines, growth factors and immune checkpoint molecules that aid tumour growth and lessen the effectiveness of CAR-T therapy.[6] As an example, cancer associated fibroblasts (CAFs) are known to inhibit T cell access to tumour cells.[1], [7], [8] To enhance CAR-T tumour infiltration, and thus the anti-cancer effect of CAR-T therapy, chemotherapy or radiotherapy can additionally be used in treatment regimens.[1] Several trials have investigated combining chemotherapy and immune checkpoint blockade to create a more hospitable immune microenvironment for CAR-T cells.[9]–[11] Due to the variety of mechanisms implicated in immunosuppression, there are many combination treatments and CAR-T designs that could be trialed *in vitro*.[1], [6]

In vitro CAR-T studies are typically conducted as 2D assays. These provide fast methods to assess the efficacy of CAR-T targeting and their cytotoxicity, but results do not always translate to 3D assays. Recently, CAR-T studies have increasingly been developed in 3D using low-adhesion well plates or hanging drop techniques, [12]–[19] with a range of readouts, such as kinetic, cytokine release, viability and activation state analysis. However, immunoassays that incorporate 3D tumour and stromal co-cultures are not widely used. With respect to off-chip CAR-T screening approaches, microfluidic technology can be effective in increasing the complexity of the 3D tumour models and the data throughput of the assays when performing combination therapy studies whilst using small sample volumes.

Miniaturized 3D immunoassays have been developed using microfluidic and lab-on-a-chip technology, [20]–[29] yet their application is still limited in relation to CAR-T studies.[30] For example, Ando *et al.* established a microfluidic assay to study the effect of hypoxic conditions on CAR-T cell behaviour.[31] Pavesi *et al.* studied T cell efficacy in an inflammatory and hypoxic microenvironment where 2D assays showed significantly greater killing by T cells in comparison to 3D microfluidic studies, emphasizing the importance of 3D models during *in vitro* modelling.[32] Therefore, miniaturized technology platforms facilitating screening of preclinical models that better mimic the challenges associated with tackling solid tumours are needed for the assessment of CAR-T therapeutic strategies, decreasing assay costs and time to results when performing advanced mechanistic studies.

In this paper, we have developed a novel proof-of-concept microfluidic immunoassay to assess CAR-T cell-mediated cytotoxicity and off-target identification on multiple triple-negative breast cancer (TNBC) -stroma co-culture spheroids, using high EGFR expressing cancer cells and low EGFR expressing normal fibroblasts or CAFs, largely neglected in *in vitro* CAR-T models[33] and implicated in the outcomes of many therapies.[8], [30], [34]. A TNBC model was chosen as TNBC makes up to 20% of breast cancer cases, is highly aggressive and lacks successful therapeutic options.[18], [35] EGFR-targeted CAR-T cells were selected as this receptor is expressed in the majority of cancer cells, including many types of TNBC, and is a promising target for the development of novel immunotherapies.[12], [18], [36] Both animal and *ex vivo* studies to date have shown that combination treatment caused a greater reduction in tumour volume and extended survival in comparison to individual monotherapies.[37]–[42] Programmed cell death protein 1 (PD-1) and programmed cell death ligand 1 (PD-L1) are responsible for the inhibition of immune responses and modulation of T cell activity.[43] The PD-1/PD-L1 pathway plays an important role in tumour escape of immune surveillance and can lessen the effectiveness of anti-cancer therapies.[43] Combination anti-PD-L1 and chemotherapy treatment for TNBC is more efficacious than individual monotherapies in terms of progression-free and overall survival.[37] Carboplatin chemotherapy is commonly used in the treatment of TNBC[38], with several trials underway to investigate various combination regimes including carboplatin and PD-1/PD-L1 inhibitors.[11], [44]

This work is the first example considering how combination treatments mimicking clinical TNBC regimens [10], [45], consisting of carboplatin chemotherapy, anti-PD-L1 therapy and CAR-T therapy, influence CAR-T killing efficiency in 3D microfluidic models. Image analysis provided quantification of cell-mediated cytotoxicity in relation to therapy-induced cell expression levels and effector-target ratio. Results showed how CAR-T killing and targeting of cancer cells was enhanced in combination studies with respect to monotherapies. This proof-of-concept work offers evidence of how the microfluidic platform and protocols can provide powerful, cost-effective and miniaturized *in vitro* assays to preclinically assess CAR-T cell therapies.

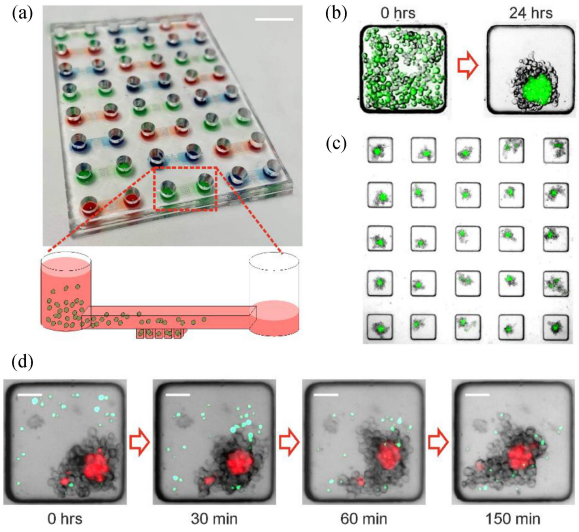

Fig. 1. Microfluidic tumour-stromal co-culture for CAR-T studies. (A) Image of the OC^{3D} Single microfluidic device used (ScreenIn3D Ltd, U.K.) with schematic showing principle of cell seeding. A single-cell suspension flows through a microchannel and cells sediment into microwell traps below the microchannel level. Scale bar = 10 mm. (B) Brightfield and fluorescence images showing spheroid formation within 24h following seeding of MDA-MB-468 (unlabelled) and CAF (green). (C) Brightfield and fluorescence image of an array of microwell traps, allowing the culture of 25 spheroids. (D) Brightfield and fluorescence images from a time-lapse experiment showing CAR-T cells (green) homing and interacting with MDA-MB-468 (unlabelled) and NHLF (red) co-culture spheroids. CAR-T cells were injected immediately prior to beginning time-lapse recording. Scale bar = 50 μm.

II. Materials and Methods

A. 3D Cell Culture in Microfluidic Devices

Cells were cultured in *OC^{3D} Single* microfluidic devices (ScreenIn3D Ltd, U.K.), consisting of an array of 24 independent culture chambers (Fig. 1(A)). Each chamber hosts 25 co-culture spheroids within ultralow-adhesion microwells (250 $\times$ 250 $\times$ 200 μm^3), which are fluidically addressable by a microfluidic channel connected by two open wells. Devices were fabricated as previously described.[46] Devices were washed using phosphate-buffered saline (PBS) and stored at 37 °C and 5% CO_2 in a humidified incubator prior to cell seeding. Cells were seeded into devices (3-7 μL at a concentration of 2-7.5$\times$ 10^6 cells/mL) to form spheroids and medium replenished every 24 to 48 hours. Cell culture details available in Supplementary Information (SI). MDA-MB-468 and stromal cells, CAF or NHLF, were seeded into devices both as 3D mono and co-cultures. Prior to the addition of CAR-T cells, DMEM was used for MDA-MDB-468 and CAF co-cultures, whilst a 50% mix of DMEM and fibroblast growth medium was used for MDA-MDB-468 and NHLF co-cultures. After CAR-T cell injection, 100% CAR-T cell media was used for all conditions.

B. CAR-T and Combination Therapy Assay

Carboplatin stock solution was diluted in cell culture media to the desired concentration for experiments (12.5-200 μM) and added for 24h to devices once cells had aggregated to form spheroids on day 1. On day 2 of culture, anti-PD-L1 antibodies

(329701, Biolegend) were injected into devices after a 1:100 dilution in culture media. On day 3 of culture, all media was removed from devices and CAR-T cells injected (3 μl at a concentration of 2.5-10x10^6/mL) and incubated for up to 72h with the spheroids. Prior to injection, cells were fluorescently labelled using dyes that were freshly prepared from CellTrace^{TM} Far Red, Bue or CFSE Proliferation Kits (Thermofisher), depending on the experimental set-up. 20uL of DMSO (Sigma) was added to a CellTrace stock vial. Cells in suspension were centrifuged and resuspended in pre-warmed PBS buffer (PBS/2%FBS) to a maximum concentration of 1 x 10^6 cells/mL 1 μL of CellTrace dye per mL of cell suspension was then added and cells incubated for 20 minutes at 37°C. After the incubation period, ice-cold quenching solution at 5 times the volume of the cell-CellTrace staining solution was added. Cells were then centrifuged and the supernatant removed. Labelled cells were resuspended in the desired volume for use in experiments. Anti-EGFR antibody (ab231, abcam) was used at a 1:200 dilution in cell culture media for EGFR blocking experiments. Anti-EGFR was added to devices on day 1 of culture for 24h before removal of all media from devices and addition of CAR-T cells for 72h. Every experiment was performed in triplicate, with at least 50 spheroids analysed per condition tested.

C. Cell Viability and Immunofluorescence

For viability, 5mg /mL fluorescein diacetate (FDA, Sigma) and 2mg /mL propidium iodide (PI, Sigma) stock solutions were freshly prepared in acetone and PBS respectively. FDA and PI were diluted in media to final concentrations of 8 μg/mL and 20 μg/mL and added to devices. Cells were incubated in the staining solution for 30 minutes at 37°C. PBS was subsequently used to wash out excess staining solution and was refreshed prior to imaging.

For quantification of EGFR and PD-L1 expression, solutions of PBSB, PBS containing 0.1% BSA (Sigma), and PBSBDT blocking solution, PBS containing 0.5% Triton-X (Fisher), 1% DMSO, 1% BSA and 1% FBS were used. All medium was removed from devices before washing with PBSB and incubation on ice for 30 minutes. PBSB was removed and 4% paraformaldehyde (PFA) added to devices for another 30 minutes. PFA was removed and devices washed again with PBSB prior to incubation with PBSBDT for 1 hour. The blocking solution was removed and primary antibodies for either EGFR, recombinant anti-EGFR antibody (ab32198, abcam), or PD-L1, purified anti-human CD274 (B7-H1, PD-L1) antibody (329701, Biolegend), were added at a 1:100 dilution for 24-48h and stored at 4°C. Devices were washed with PBSB and incubated at room temperature for 10 minutes before the addition of secondary antibodies in a 1:200 ratio. Goat anti-Mouse Alexa Fluor 633 Secondary Antibody (Thermofisher) was added for PD-L1 quantification and Goat anti-Rabbit Alexa Fluor 633 Secondary Antibody (Thermofisher) was added for EGFR quantification. Secondary antibodies were incubated in devices for 2 hours at room temperature before washing steps and imaging.

D. Statistical Analysis

Statistical analysis was carried out with GraphPad Prism 8.1.2 (GraphPad Software, Inc., San Diego, CA). All data is presented as mean $\pm$ standard deviation, unless otherwise stated, using bar graphs or scatter plots. T-tests were used for the comparison of two variables. For comparison of multiple variables, one-way analysis of variance (ANOVA) with Bonferroni multiple comparison tests were conducted. Differences between groups were considered to be significant at a P value of <0.05. At least 50 spheroids of similar size were considered for statistical analysis per condition tested.

E. Microscopy Setup and Image Analysis

Cultures were imaged via bright-field and epifluorescence microscopy using an inverted microscope (Axio Observer Z1, Zeiss) connected to an Orca Flash 4.0 camera (Hamamatsu). For real-time imaging experiments, devices were kept in a temperature and humidity controlled stage top incubator (OKOLAB, Italy) for automated imaging overnight at 37°C at 94% relative humidity with a gas flow rate of 0.1 l/min. Image analysis was performed using ZEN Blue and Fiji to measure spheroid area and to count CAR-T cells. Details available in SI.

III. Results

To establish a co-culture system for EGFR-specific CAR-T-mediated cytotoxicity, we selected MDA-MB-468 breast cancer cells for their reportedly high expression of EGFR.[47]–[49]. We also chose two stromal cell types with low level expression of the EGFR receptor: immortalized cancer-associated fibroblasts (CAF) from a breast tumour and normal human lung fibroblasts (NHLF). EGFR expression levels were consistent with previous reports, showing that MDA-MB-468 expression of EGFR was approximately 4 times greater than in CAF and 5 times greater than in NHLF (Figure S1 in SI), providing positive and negative targets of EGFR-specific CAR-T cells.

A. Assessment of EGFR Specificity of CAR-T in 2D

Tests were first performed in 2D to assess the cytotoxic activity of CAR-T cells towards the EGFR target. For this, monocultures of MDA-MDB-468 were established in 96-well plates (Figure S1 in SI). Assays investigating the effect of varying effector to target (E:T) ratio, testing 1:2, 1:1 and 5:1 E:T ratios, showed that the number of live MDA-MB-468 cells decreased with increasing E:T ratio after 72h incubation with CAR-T cells. The number of CAR-T cells remained constant throughout the duration of the assay. Even at an unfavourable 1:2 E:T ratio, CAR-T elicited a significant cytotoxic effect on cancer cells.

B. 3D Co-Culture Models

Aiming to validate cost-effective 3D assays that minimise usage of CAR-T material, microfluidic 3D experiments were

designed to obtain a 1:10 E:T to visualise CAR-T interaction with the cancer spheroid model (Fig. 1(D)). The high specificity of the CAR-T cells used meant that E:T ratios 10 to 100 times lower than typical values for *in vitro* assays could be used to produce statistically significant cytotoxicity. Throughout the development of this assay, protocols were refined to use as few as 7500 T cells/injection in each culture chamber, achieving a uniform distribution of CAR-Ts in the 25 microwells (approx. 20 CAR-Ts per 200 cancer scells).

This outcome is evidence of the miniaturization capabilities of the platform and its potential benefit for future assays with patient biopsy tissue.

MDA-MB-468 and the two fibroblasts were seeded at a 1:1 ratio in *OC^{3D} Single* microfluidic devices, hosting 24 array chambers (Fig. 1(A)). Due to the ultra-low adhesion conditions, cells formed a spheroid within 24 hours with CAF aggregating together in regions within the co-culture spheroid, forming CAF 'islands', as previously reported in other tumour-stroma models,[8] (Fig. 1(B)). Each microfluidic chamber enables the simultaneous formation and culture of 25 spheroids. To keep cell numbers similar in each condition tested, monoculture cancer spheroids resulted in 50-70 μm in radius, monoculture fibroblast spheroids resulted in 20-30 μm in radius and co-culture spheroids in 30-50 μm in radius (Fig. 1(C)). After a 24 hours spheroid formation, CAR-T cells were injected, obtaining a 1:10 CAR-T to cancer cell ratio, and immediately migrated towards the spheroids. Within a 3 hours window, each CAR-T cell could be seen interacting with the spheroid mass (Fig. 1(D)) (MovieS1 in SI).

C. Assessment of CAR-T Targeting and Cytotoxicity

Microfluidic 3D cultures were set up to test both the CAR-T targeting specificity and their mediated cytotoxicity on MDA-MB-468 and fibroblast spheroids, both alone and as co-cultures (Fig. 2). CAR-T cells were incubated for 72 hours prior to imaging and viability staining.

Two outcomes resulted from this assay: first, CAR-T induced disaggregation of MDA-MB-468 spheroids over the first few hours of incubation, irrespectively of whether monoculture and co-culture spheroids were used. No significant change to the area of CAF monoculture spheroids incubated with CAR-T cells was observed (Fig. 2(C)). Lastly, an elevated marker of cell death (intensity from PI signal) was obtained for MDA-MB-468 spheroid monocultures and MDA-MB-468-CAF and MDA-MB-468-NHLF spheroid co-cultures with respect to controls after 72 hours CAR-T incubation (Fig. 2(D)). Quantification of cytotoxicity was performed by obtaining the PI area from the normalized fluorescence image and plotting this as a ratio over the total brightfield area of the tumour spheroid. It should be noted that due to the washing steps involved in the staining process, dead cancer cells that had become detached from the main tumour bulk were washed out from microwells and, thus, could not included in the total dead spheroid area. No significant change in cell death was detected for CAF monoculture spheroids after 72h CAR-T treatment. This data suggests that CAR-T cells predominantly targeted EGFR high-expressing cells. To further confirm this finding, image analysis was performed to quantify PI signal co-localization with cancer cells, fibroblasts or CAR-T cells (Fig. 2(E)). For NHLF and CAF co-cultures, the percentage of PI signal co-localised to cancer cells was quantified as $88.6 \pm 1.4\%$ and $91.7 \pm 1.9\%$, respectively (Fig. 2(F)). Considering the lack of cell death obtained from fibroblast spheroid mono-cultures (both CAF and NHLF, Fig. 2(D)), the results are indicative of high level, on-target specificity of the CAR-T cells. CAR-T numbers remained comparable over the duration of the 3D assay (Fig. 2(G)).

To determine whether these cytotoxic effects were produced only by CAR-T cells binding to the EGFR, an anti-EGFR antibody was incubated with MDA-MB-468 and CAF spheroid monocultures for 24 hours prior to CAR-T cell injection (Figure S2) and washed out. Cultures were subsequently incubated for 72 hours with CAR-T cells. The EGFR antibodies did not cause any significant change in spheroid area or viability when administered alone with respect to controls (Figure S2C-D in SI). However, when present with spheroid co-cultures and CAR-T cells, they prevented both MDA-MD-468 spheroid disaggregation and cell death (measured by PI signal) (Figure S2C-D in SI). These results confirmed CAR-T cell-mediated cytotoxicity and target specificity through EGFR recognition and that this effect could be neutralized with administration of an anti-EGFR antibody.

D. Combination Therapy

Having characterised the effects and the efficacy of CAR-T administration alone, further studies were performed to assess the outcomes when CAR-T was combined with other anticancer therapies (Fig. 3). Based on clinical TNBC therapy regiments, carboplatin and anti-PD-L1 antibody treatments were selected for use in conjunction with CAR-T therapy. For this, after spheroid formation, cells were exposed to carboplatin for 24h, after which all media was removed and anti-PD-L1 antibodies were incubated with the spheroids into devices for another 24h period. After this, all medium was removed and CAR-T cells added to the devices for 72h.

Prior to this, MDA-MB-468 spheroid monoculture's sensitivity to carboplatin was tested to identify the EC50 and chose the optimum chemotherapeutic dose that would produce a mild chemotoxic effect, maintaining acceptable spheroid viability and aggregation in order to assess any synergistic effects produced by CAR-T cells in all possible conditions. An EC50 of 28 μM was obtained (Figure S3B in SI).

Brightfield and live spheroid area were found to decrease with increasing carboplatin concentration, whilst PI area and spheroid disaggregation increased with greater doses (Figure S3C-E). Accurate area values were not attainable for spheroids exposed to higher drug concentrations due to extreme disaggregation. The concentration of carboplatin used for combination treatments was selected as 12.5 μM, which produced a non-negligible but mild cytotoxic effect (Fig. 3).

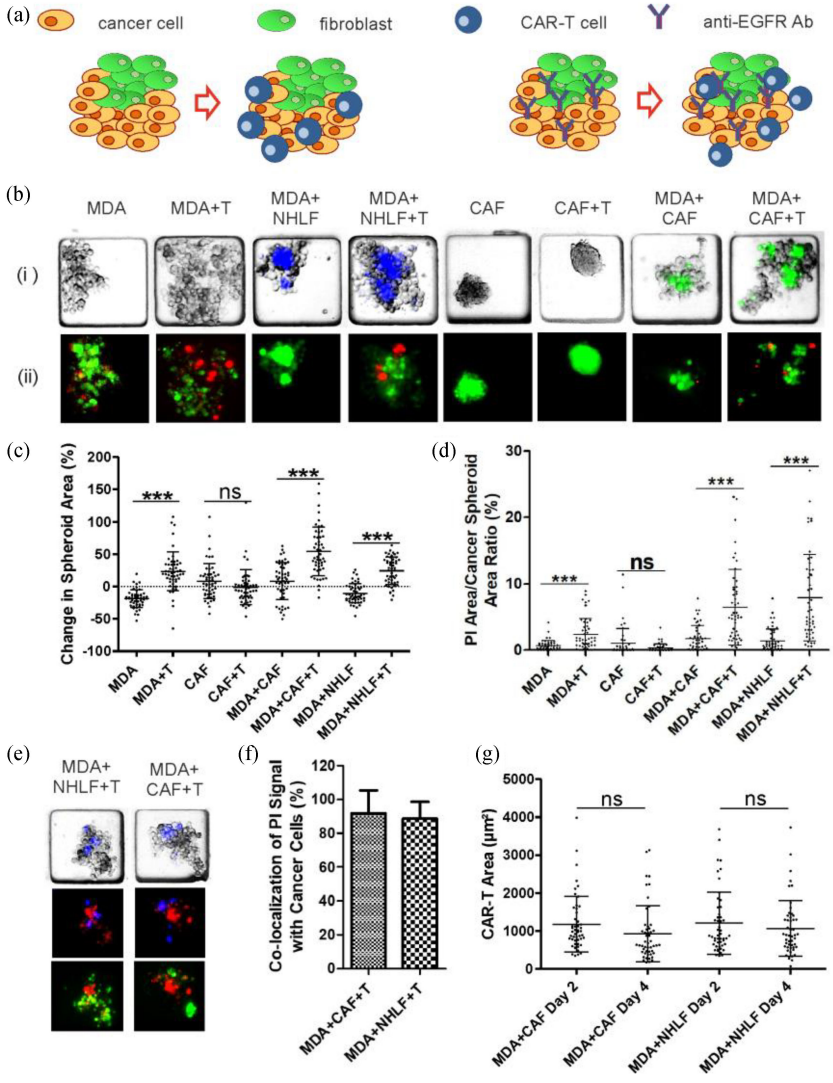

Fig. 2. CAR-T targeting specificity and cytotoxicity in mono- and co-cultures. (a) Schematic of experimental set-up showing cancer cell (yellow) and fibroblast (green) co-culture spheroids treated with CAR-T cells (blue) and anti-EGFR antibodies. (b) Representative images of spheroids from MDA-MB-468 and CAF monocultures and MDA-MB-468 spheroids in co-culture with CAF (green) and NHLF (blue) after 72h CAR-T incubation. CAF were transfected with GFP, thus viability staining using FDA was not performed. NHLF were labelled with CellTrace Blue to allow viability staining with FDA (green). (i) Brightfield and fluorescence images. (ii) Fluorescence images obtained after staining with FDA (green) and PI (red). For CAF mono- and co-cultures, no FDA staining was performed due to CAF transfection with GFP. In these images, the green signal indicates presence of CAF and not live cells and only staining with PI was performed (red). (c) Plot of percentage change in spheroid area from day 2 to day 5 of culture (n=50). (d) Plot of PI area signal normalised to spheroid area (n=50). (e) Representative brightfield and fluorescence images of MDA-MB-468 (unlabelled) in co-culture with NHLF/CAF (green) after 72h of CAR-T (blue) incubation and stained with PI (red). (f) Plot of percentage of PI signal co-localised only with unlabelled cancer cells (n=50). (g) Plot of area representative of CAR-T cell coverage in microfluidic devices over time, n=50. MDA=MDA-MB-468, T= CAR-T cells.

Results from combination assays on MDA-MB-468 spheroids showed a statistically significant reduction in spheroid areas when chemotherapy was administered alone and in combination with anti-PD-L1 and CAR-T cells (Fig. 3(C)). The greatest reduction in cancer cell spheroid area was found to occur when all therapies were combined. A significant increase in the percentage cell death of the spheroid was only recorded for conditions that included carboplatin, given alone or in combinations (Fig. 3(D)). In the absence of chemotherapy treatment, no statistically significant changes could be detected between CAR-T treatment alone and CAR-T and anti-PD-L1 therapy, suggesting a minor effect of the checkpoint inhibitor in these experiments. Following these studies, the same therapy conditions were also tested against CAF and MDA-MB-468 spheroid co-cultures. (Fig. 4).

Consistent with the results obtained from MDA-MDB-468 monoculture conditions, the spheroid area was significantly reduced when chemotherapy was administered alone and in combinations with CAR-T and anti-PD-L1 treatment and CAR-T (Fig. 4(C)). The largest reduction in spheroid mass was recorded where chemotherapy, anti-PD-L1 and CAR-T were combined. CAFs, expressing low levels of EGFR, were resistant to all

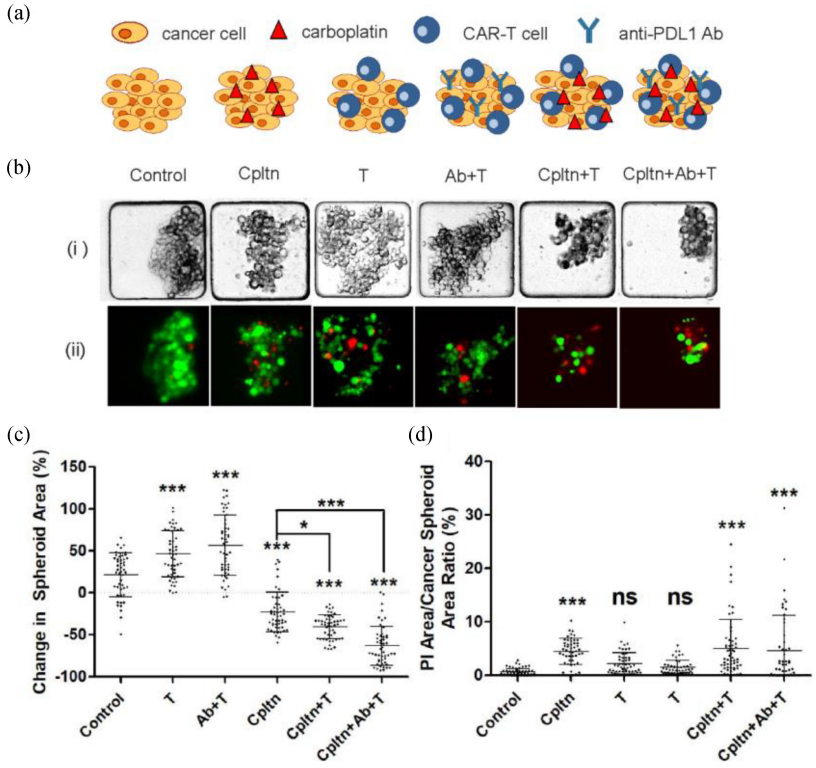

Fig. 3. Analysis of the effects produced by combination therapies in MDA-MB-468 spheroid monocultures. (a) Schematic of the different combination therapy modalities used. (b) Representative (i) brightfield and (ii) fluorescence images of MDA-MB-468 monoculture spheroids on day 6, after viability staining with FDA (green) and PI (red). (c) Plot of the percentage change in spheroid area, measured from brightfield images, from day 1 to day 6 (n=50). (d) Plot of PI area signal normalised to spheroid area (n=50). Cpltn = carboplatin chemotherapy, Ab = Anti-PD-L1 antibodies, T= CAR-T cells.

combination therapy tested (Fig. 4(D)), showing no statistically significant differences in spheroid shape or size when in co-culture. A statistically significant increase in dead cancer cells was recorded for chemotherapy alone and in combination with CAR-T and anti- PD-L1 treatments (Fig. 4(E)). The combination of anti-PD-L1 treatment with CAR-Ts did not show an increase in cancer cell death, with the chemotherapy treatment being the main discriminant for enhancing the cytotoxic effects of CAR-T cells. Also for combination studies, the majority of the PI signal (on average 89.63%) originated from cancer cells in comparison to carboplatin monotherapy (68.94%), demonstrating the on-target specificity of the CAR-T under investigation (Fig. 4(F)).

Increased cell death ($^{*}P < 0.01$) and further reduction in cancer spheroid area ($^{****}P < 0.0001$) were observed in monocultures in comparison to CAF co-cultures treated with combined CAR-T, chemotherapy and checkpoint blockade therapy (Figure S4 in SI). Previous work with cancer cell and CAF co-cultures has indicated potential benefit to cancer cells when co-cultured with CAFs. [8] As fibroblasts appear resistant to all treatment combinations, this could suggest that CAFs are potentially beneficial to cancer cell survival or could offer a degree of physical protection to cancer cells from CAR-T cell killing.

Some chemotherapies have been reported in the literature to increase tumour cell expression of EGFR [50]–[52] and PD-L1 [53]–[55] for several cancer types. Thus, the levels of EGFR and PD-L1 expression were assessed in the microfluidic for MDA-MB-468 monoculture spheroids after exposure to carboplatin in order to better interpret the results from the 3D assays (Fig. 5). Spheroids were treated with carboplatin for 24h after formation and subsequently fixed and stained for PD-L1 and EGFR to quantify expression levels caused by chemotherapy.

IV. Discussion

This proof-of-concept work provides an example as to how miniaturization through lab-on-chip technologies can be utilized to augment output data when using limited resources. Due to the high selective toxicity of the CAR-T cells and the miniaturization capability of the microfluidic platform used in this work, the E:T ratio could be reduced to far lower values than is typical for conventional *in vitro* studies,[19], [56], [57] whilst still eliciting significant cytotoxic effects on the 3D tumour model. Continuous refinement of cell seeding protocols during this work has resulted in the ability to perform over a hundred 3D CAR-T assays (each with 25 technical repeats) using just 1 million cells. This offers the opportunity to develop material-saving and cost-effective assays for the rapid assessment of CAR-T efficacy and on-target specificity for *in vitro* CAR-T studies.

The microfluidic platform offers the potential to expand these studies to other adoptive cell therapy strategies for solid tumours, depicting a variety of reconstructed TME conditions in 3D, favouring the development of mechanistic studies for preclinical

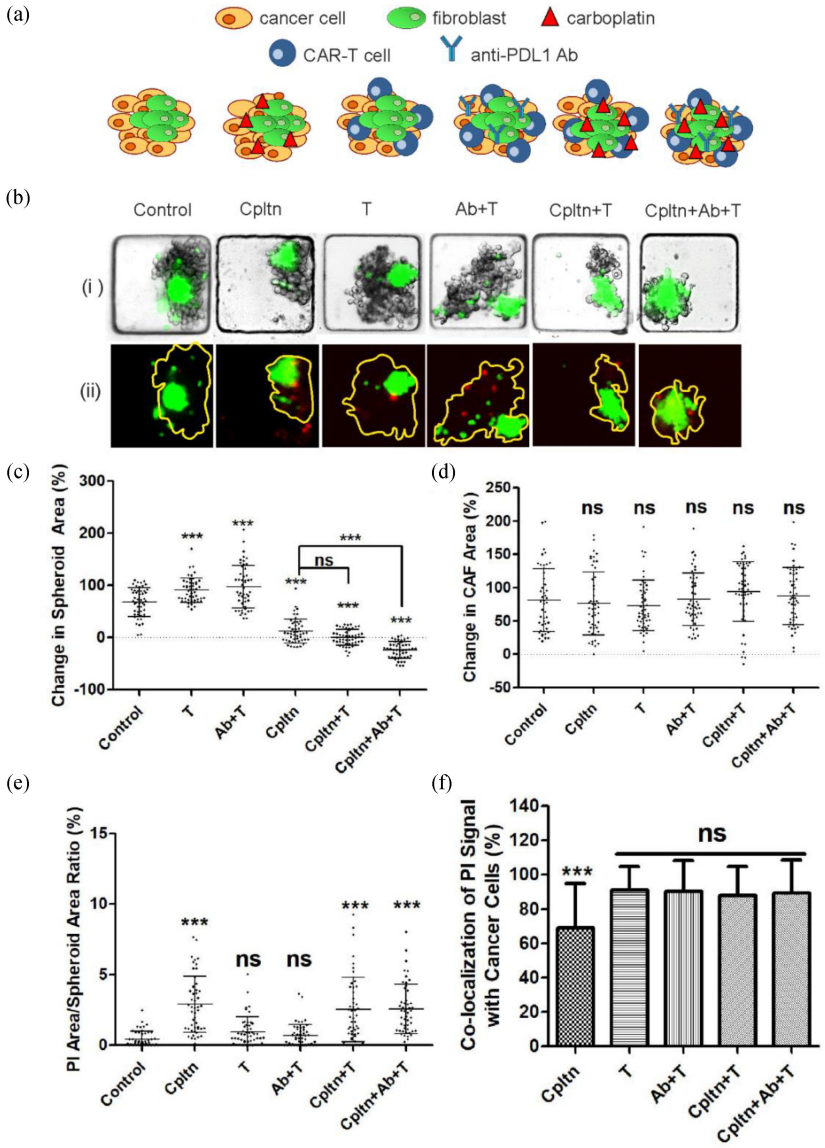

Fig. 4. Analysis of the effects produced by combination therapies in MDA-MDB-468 and CAF spheroid co-cultures. (A) Schematic of the different combination therapy modalities used. (B) Representative brightfield and fluorescence images (i) of MDA-MB-468 and CAF (green) co-culture spheroids on day 6, and (ii) after viability staining with PI (red). Yellow outline represents spheroid area. (C) Plot of the percentage change in spheroid area from day 1 to 6, measured from brightfield images (n=50). (D) Plot of CAF spheroid area on day6 of culture extracted from co-culture experiments (n=50). (E) Plot of PI area signal normalised to spheroid area (n=50). (F) Plot of percentage of PI signal co-localised only with unlabelled cancer cells (n=30). Cpltn = carboplatin chemotherapy, Ab = Anti-PD-L1 antibodies, T= CAR-T cells.

in vitro assessment prior to *in vivo* studies. This is of particular benefit when determining the efficacy of anti-cancer agents due to the protection provided to tumour cells by the stromal tissue and, in particular, CAFs. To overcome this challenge, CAR-T cells targeting particular CAF proteins could be utilized first to deconstruct the TME prior to tumour targeting treatment. For example, CAR-T targeting fibroblast activation protein, overexpressed by CAF, have been developed and studied in several pre-clinical and clinical studies showing anti-tumour effects. [58]

In this work, CAR-T cells were shown to pull apart the tumour cell aggregate. These findings highlight the importance of considering a variety of readouts in order to fully assess treatment efficacy in 3D and shows how the platform can offer novel insights into CAR-T and tumour cell interactions. Chemotherapy treatment was shown not to be cancer cell specific when applied as a monotherapy. However, when combined with CAR-T cell treatment, the cancer cell specificity of the combination treatment was enhanced when compared to carboplatin monotherapy. In addition, statistically greater disaggregation was recorded for combination carboplatin, anti-PD-L1 therapy and CAR-T treatment in comparison to carboplatin monotherapy for both cancer cell monocultures and co-cultures with CAF. These findings demonstrate the potential of microtechnologies to deliver valuable preclinical data in solid tumour immunotherapy investigations.

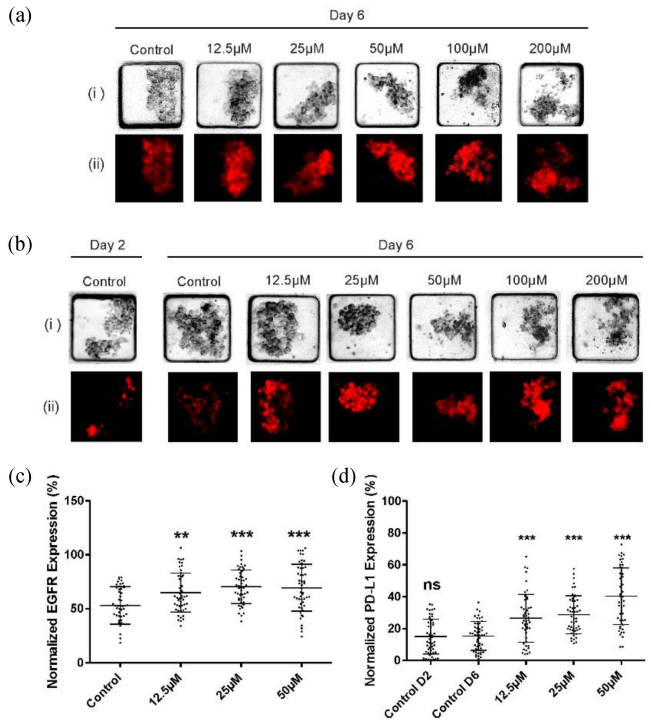

Fig. 5. Effect of carboplatin treatment on PD-L1 and EGFR expression levels in MDA-MB-468 spheroids. (A) Representative (i) brightfield and (ii) fluorescent images of MDA-MDB-468 spheroid monocultures stained with anti-EGFR antibody (red) following carboplatin incubation. (B) Representative (i) brightfield and (ii) fluorescent images of MDA-MDB-468 monocultures stained with anti-PD-L1 antibody (red) following carboplatin incubation. (C) Plot of EGFR expression normalized to spheroid area (n=50). (D) Plot of PD-L1 expression normalized to spheroid area on day 6 of culture (n=50). MDA = MDA-MB-468, D2 = Day 2, D6 = Day 6.

2D assays commonly study immune cell function and cytotoxicity, measuring cytokines or chemokines present in the culture media, but fail to recapitulate many aspects of the 3D microenvironment. Previous studies in microfluidics have explored the effects of varying oxygen concentration on immune cell function against solid tumours, where gel-embedded tumour aggregates were utilised that did not include the stromal component.[32] Unlike alternative immunoassays, this platform does not require connection to tubing, is easy to use and has potential for integration with robotic dispensers. Furthermore, the multichannel design of this system means that multiple independent assays can be conducted on a single chip. Here, we have focussed our attention on investigating readouts that can provide insights into T-cell interactions with solid tumours when testing immunotherapeutic strategies. In the future, the miniaturization yet medium-throughput capabilities of the platform could be used to investigate the efficacy and specificity of other adoptive cell therapies in combination with numerous other anti-cancer agents to identify the optimum regiment for a specific patient, providing a flexible platform for precision medicine using patient derived tissue.[46]

Chemotherapy exposure was found to trigger an increase in the expression of EGFR (Fig. 5(A)–(B)) as well as PD-L1 (Fig. 5(C)–(D)), for all carboplatin concentration values tested with respect to controls. We would speculate that EGFR and PD-L1 upregulation by chemotherapy is a result of stress response mechanisms, such as IFN or MYC signalling. This reaction to chemotherapy explained the enhanced CAR-T cell-mediated cytotoxicity observed in the combination therapy conditions, as increased level of EGFR increased the likelihood of CAR-T cell binding. Even if PD-L1 expression levels were increased, this had a secondary effect on CAR-T efficacy with respect to overexpression of the target. Overall, these results show how a combination of these agents was able to elicit a more powerful anti-cancer response in comparison to monotherapies. In future, the effect of carboplatin on cancer cell cytokine secretion could be also investigated to identify the release of immunosuppressive molecules that could impede CAR-T cell cytotoxicity. In addition, other aspects of the TME can be readily incorporated in the platform, such as different immune cells to study immunosuppressive effects or the ability create larger 3D cancer models to develop hypoxia as a further element for studying T-cell inhibition or chemo-resistance.

V. Conclusion

In this work, a novel microfluidic TNBC immunoassay was developed to evaluate CAR-T cell-mediated cytotoxicity and target specificity against the EGF receptor using tumour cells co-cultured with stromal cells in 3D. This is the first report showing a miniaturised assay for the assessment of chemotherapy, biologics and cell therapy studies in a 3D solid tumour platform. CAR-T cells rapidly targeted, disaggregated and killed cancer cells without significant cytotoxicity to the 3D stromal mass. This effect could be neutralised by blocking EGFR recognition by CAR-T. The cytotoxic effects of EGFR targeting CAR-Ts was demonstrated to be most pronounced when spheroids were pre-treated with chemotherapy, as this induced upregulation of EGFR and PD-L1 expression by tumour cells. The platform enabled quantification of readouts, including on-target specificity, offering powerful solutions for in vitro assessment of CAR-T cell therapies.

VI. Supplementary Materials

We provide details of cell culture conditions, image and data analysis, in addition to experiments that evaluate results from supplementary 2D and 3D assays, and a video of time-lapse experiments.

References

[1] S. Srivastava and S. R. Riddell, "Chimeric antigen receptor T cell therapy: Challenges to bench-to-bedside efficacy," (in English), *J. Immunol., (Baltimore, Md. : 1950)*, vol. 200, no. 2, pp. 459–468, 2018, doi: 10.4049/jimmunol.1701155.

[2] N. Schaft, "The landscape of CAR-T cell clinical trials against solid Tumors—A comprehensive overview," *Cancers*, vol. 12, no. 9, 2020, Art. no. 2567, [Online]. Available: https://www.mdpi.com/2072-6694/12/9/2567

[3] R. P. Harrison, E. Zylberberg, S. Ellison, and B. L. Levine, "Chimeric antigen receptor–T cell therapy manufacturing: Modelling the effect of offshore production on aggregate cost of goods," *Cytotherapy*, vol. 21, no. 2, pp. 224–233, 2019, doi: 10.1016/j.jcyt.2019.01.003.

[4] T. R. Abreu, N. A. Fonseca, N. Gonçalves, and J. N. Moreira, "Current challenges and emerging opportunities of CAR-T cell therapies," *J. Controlled Release*, vol. 319, pp. 246–261, 2020, doi: 10.1016/j.jconrel.2019.12.047.

[5] A. Titov *et al.*, "The biological basis and clinical symptoms of CAR-T therapy-associated toxicites," (in English), *Cell Death Dis.*, vol. 9, no. 9, 2018, Art. no. 897, doi: 10.1038/s41419-018-0918-x.

[6] F. Marofi *et al.*, "CAR T cells in solid tumors: Challenges and opportunities," *Stem Cell Res. Ther.*, vol. 12, no. 1, 2021, Art. no. 81, doi: 10.1186/s13287-020-02128-1.

[7] A. Santi, F. G. Kugeratski, and S. Zanivan, "Cancer associated fibroblasts: The architects of stroma remodeling," *Proteomics*, vol. 18, no. 5-6, 2018, Art. no. 1700167, doi: 10.1002/pmic.201700167.

[8] E. J. Kay *et al.*, "PYCR1-dependent proline synthesis in cancer-associated fibroblasts is required for the deposition of pro-tumorigenic extracellular matrix," *Nature Metabolism*, to be published.

[9] S. Toulouie, G. Johanning, and Y. Shi, "Chimeric antigen receptor T-cell immunotherapy in breast cancer: Development and challenges," *J. Cancer*, vol. 12, no. 4, pp. 1212–1219, 2021, doi: 10.7150/jca.54095.

[10] Z. Li, Y. Qiu, W. Lu, Y. Jiang, and J. Wang, "Immunotherapeutic interventions of triple negative breast cancer," *J. Transl. Med.*, vol. 16, no. 1, 2018, Art. no. 147, doi: 10.1186/s12967-018-1514-7.

[11] I. Kim, K. Sanchez, H. L. McArthur, and D. Page, "Immunotherapy in triple-negative breast cancer: Present and future," *Curr. Breast Cancer Rep.*, vol. 11, no. 4, pp. 259–271, 2019, doi: 10.1007/s12609-019-00345-z.

[12] Y. Li *et al.*, "The targeting effect of cetuximab combined with PD-L1 blockade against EGFR-expressing tumors in a tailored CD16-CAR T-Cell reporter system," *Cancer Investigation*, vol. 39, no. 4, pp. 285–296, 2021, doi: 10.1080/07357907.2021.1894570.

[13] R. Zhou *et al.*, "CAR T cells targeting the tumor MUC1 glycoprotein reduce triple-negative breast cancer growth," *Front. Immunol.*, vol. 10, no. 1149, 2019, doi: 10.3389/fimmu.2019.01149.

[14] G. Liu *et al.*, "CXCR2-modified CAR-T cells have enhanced trafficking ability that improves treatment of hepatocellular carcinoma," *Eur. J. Immunol.*, vol. 50, no. 5, pp. 712–724, 2020, doi: 10.1002/eji.201948457.

[15] S. Herter *et al.*, "A novel three-dimensional heterotypic spheroid model for the assessment of the activity of cancer immunotherapy agents," *Cancer Immunol., Immunotherapy*, vol. 66, no. 1, pp. 129–140, 2017, doi: 10.1007/s00262-016-1927-1.

[16] A. B. Bergeron and H. J. Gitschier, "CAR-T cell screening in tumor spheroids using corning spheroid microplates and the KILR cytotoxicity assay application note," M.S. Corning Incorporated, Life Sciences, Kennebunk, Maine, 2017.

[17] L. Wallstabe *et al.*, "ROR1-CAR T cells are effective against lung and breast cancer in advanced microphysiologic 3D tumor models," *JCI Insight*, vol. 4, no. 18, 2019, Paper e126345, doi: 10.1172/jci.insight.126345.

[18] Y. Liu *et al.*, "EGFR-specific CAR-T cells trigger cell lysis in EGFR-positive TNBC," *Aging*, vol. 11, 2019, Art. no. 11054, doi: 10.18632/aging.102510.

[19] P. Dillard, H. Köksal, E.-M. Inderberg, and S. Wälchli, "A spheroid killing assay by CAR T cells," *J. Vis. Exp.*, vol. 142, 2018, Art. no. e58785, doi: 10.3791/58785.

[20] A. E. Christakou, M. Ohlin, B. Önfelt, and M. Wiklund, "Ultrasonic three-dimensional on-chip cell culture for dynamic studies of tumor immune surveillance by natural killer cells," *Lab Chip*, vol. 15, no. 15, pp. 3222–3231, 2015, doi: 10.1039/C5LC00436E.

[21] J. M. Ayuso *et al.*, "Evaluating natural killer cell cytotoxicity against solid tumors using a microfluidic model," *Oncoimmunology*, vol. 8, no. 3, 2019, Art. no. 1553477, doi: 10.1080/2162402X.2018.1553477.

[22] J. M. Ayuso *et al.*, "Microfluidic tumor-on-a-chip model to evaluate the role of tumor environmental stress on NK cell exhaustion," *Sci. Adv.*, vol. 7, 2021, Paper eabc2331.

[23] S. W. L. Lee *et al.*, "Characterizing the role of monocytes in T cell cancer immunotherapy using a 3D microfluidic model," *Front. Immunol.*, vol. 9, 2018, Art. no. 416, doi: 10.3389/fimmu.2018.00416.

[24] J. Lee, S. E. Kim, D. Moon, and J. Doh, "A multilayered blood vessel/tumor tissue chip to investigate T cell infiltration into solid tumor tissues," *Lab Chip*, 2021, vol. 21, no. 11, pp. 2142–2152, 2021, doi: 10.1039/d1lc00182e.

[25] D. Di Mascolo *et al.*, "Nanoformulated zoledronic acid boosts the vδ2 T cell immunotherapeutic potential in colorectal cancer," *Cancers (Basel)*, vol. 12, no. 1, 2019, Art. no. 104, doi: 10.3390/cancers12010104.

[26] V. Charwat *et al.*, "Monitoring dynamic interactions of tumor cells with tissue and immune cells in a Lab-on-a-Chip," *Anal. Chem.*, vol. 85, no. 23, pp. 11471–11478, 2013, doi: 10.1021/ac4033406.

[27] J. P. Layer *et al.*, "Amplification of N-Myc is associated with a T-cell-poor microenvironment in metastatic neuroblastoma restraining interferon pathway activity and chemokine expression," *Oncoimmunology*, vol. 6, no. 6, 2017, Art. no. e1320626, doi: 10.1080/2162402X.2017.1320626.

[28] S. C. Chen, P. C. Wu, C. Y. Wang, and P. L. Kuo, "Evaluation of cytotoxic T lymphocyte-mediated anticancer response against tumor interstitium-simulating physical barriers," *Sci. Rep.*, vol. 10, no. 1, 2020, Art. no. 13662, doi: 10.1038/s41598-020-70694-8.

[29] G. Ronteix *et al.*, "A multiscale immuno-oncology on-Chip system (MIOCS) establishes that collective T cell behaviors govern tumor regression," *bioRxiv*, 2021, doi: 10.1101/2021.03.23.435334.

[30] K. Paterson, S. Zanivan, R. Glasspool, S. B. Coffelt, and M. Zagnoni, "Microfluidic technologies for immunotherapy studies on solid tumours," *Lab Chip*, vol. 21, no. 12, pp. 2306–2329, 2021, doi: 10.1039/d0lc01305f.

[31] Y. Ando *et al.*, "Evaluating CAR-T cell therapy in a hypoxic 3D tumor model," *Adv. Healthcare Mater.*, vol. 8, no. 5, 2019, Art. no. 1900001, doi: 10.1002/adhm.201900001.

[32] A. Pavesi *et al.*, "A 3D microfluidic model for preclinical evaluation of TCR-engineered T cells against solid tumors," *JCI Insight*, vol. 2, no. 12, 2017, Art. no. e89762, doi: 10.1172/jci.insight.89762.

[33] A. Rodriguez-Garcia, A. Palazon, E. Noguera-Ortega, D. J. Powell Jr., and S. Guedan, "CAR-T cells hit the tumor microenvironment: Strategies to overcome tumor escape," *Front. Immunol.*, vol. 11, 2020, Art. no. 1109, doi: 10.3389/fimmu.2020.01109.

[34] Q. Ping *et al.*, "Cancer-associated fibroblasts: Overview, progress, challenges, and directions," *Cancer Gene Ther.*, vol. 28, pp. 984–999, 2021, doi: 10.1038/s41417-021-00318-4.

[35] K. H. Jung *et al.*, "Targeted therapy of triple negative MDA-MB-468 breast cancer with curcumin delivered by epidermal growth factor-conjugated phospholipid nanoparticles," *Oncol. Lett.*, vol. 15, no. 6, pp. 9093–9100, Jun. 2018, doi: 10.3892/ol.2018.8471.

[36] J. Wykosky, T. Fenton, F. Furnari, and W. K. Cavenee, "Therapeutic targeting of epidermal growth factor receptor in human cancer: Successes and limitations," *Chin. J. Cancer*, vol. 30, no. 1, pp. 5–12, 2011, doi: 10.5732/cjc.010.10542.

[37] A. Bassez *et al.*, "A single-cell map of intratumoral changes during anti-PD1 treatment of patients with breast cancer," *Nature Med.*, vol. 27, no. 5, pp. 820–832, 2021, doi: 10.1038/s41591-021-01323-8.

[38] M. Gao, T. Wang, L. Ji, S. Bai, L. Tian, and H. Song, "Therapy with carboplatin and anti-pd-1 antibodies before surgery demonstrates sustainable anti-tumor effects for secondary cancers in mice with triple-negative breast cancer," *Front. Immunol.*, vol. 11, no. 366, 2020, doi: 10.3389/fimmu.2020.00366.

[39] S. Srivastava *et al.*, "Immunogenic chemotherapy enhances recruitment of CAR-T cells to lung tumors and improves antitumor efficacy when combined with checkpoint blockade," (in English), *Cancer Cell*, vol. 39, pp. 193–208, 2021.

[40] L. A. Emens and G. Middleton, "The interplay of immunotherapy and chemotherapy: Harnessing potential synergies," *Cancer Immunol. Res.*, vol. 3, no. 5, pp. 436–443, 2015, doi: 10.1158/2326-6066.CIR-15-0064.

[41] C. Bailly, X. Thuru, and B. Quesnel, "Combined cytotoxic chemotherapy and immunotherapy of cancer: Modern times," *NAR Cancer*, vol. 2, no. 1, Art. no. zcaa002, 2020, doi: 10.1093/narcan/zcaa002.

[42] C. A. Hartl *et al.*, "Combination therapy targeting both innate and adaptive immunity improves survival in a pre-clinical model of ovarian cancer," *J. Immunotherapy Cancer*, vol. 7, no. 1, 2019, Art. no. 199, doi: 10.1186/s40425-019-0654-5.

[43] Y. Han, D. Liu, and L. Li, "PD-1/PD-L1 pathway: Current researches in cancer," *Amer. J. Cancer Res.*, vol. 10, no. 3, pp. 727–742, 2020. [Online]. Available: https://pubmed.ncbi.nlm.nih.gov/32266087

[44] K. Oualla *et al.*, "Immunotherapeutic approaches in triple-negative breast cancer: State of the art and future perspectives," *Int. J. Breast Cancer*, vol. 2020, 2020, Art. no. 8209173, doi: 10.1155/2020/8209173.

[45] K. Mediratta, S. El-Sahli, V. D'Costa, and L. Wang, "Current progresses and challenges of immunotherapy in triple-negative breast cancer," *Cancers (Basel)*, vol. 12, no. 12, 2020, Art. no. 3529, doi: 10.3390/cancers12123529.

[46] T. Mulholland *et al.*, "Drug screening of biopsy-derived spheroids using a self-generated microfluidic concentration gradient," *Sci. Rep.*, vol. 8, no. 1, pp. 1–17, 2018, doi: 10.1038/s41598-018-33055-0.

[47] A. El Guerrab, M. Bamdad, F. Kwiatkowski, Y.-J. Bignon, F. Penault-Llorca, and C. Aubel, "Anti-EGFR monoclonal antibodies and EGFR tyrosine kinase inhibitors as combination therapy for triple-negative breast cancer," *Oncotarget*, vol. 7, no. 45, pp. 73618–73637, 2016, doi: 10.18632/oncotarget.12037.

[48] H. Hossein-Nejad-Ariani, E. Althagafi, and K. Kaur, "Small peptide ligands for targeting EGFR in triple negative breast cancer cells," *Sci. Rep.*, vol. 9, no. 1, 2019, Art. no. 2723, doi: 10.1038/s41598-019-38574-y.

[49] M. K. Wendt *et al.*, "The antitumorigenic function of EGFR in metastatic breast cancer is regulated by expression of Mig6," *Neoplasia*, vol. 17, no. 1, pp. 124–133, 2015, doi: 10.1016/j.neo.2014.11.009.

[50] Z. Hao, C. Tian, F. Yang, and J. Zhang, "Correlation between expression of epidermal growth factor receptor and adverse reactions after chemotherapy of advanced non-small-cell lung cancer," *Pakistan J. Med. Sci.*, vol. 31, no. 5, pp. 1115–1120, Sep./Oct 2015, doi: 10.12669/pjms.315.7939.

[51] N. O'Donovan and J. Crown, "EGFR and HER-2 antagonists in breast cancer," *Anticancer Res.*, vol. 27, pp. 1285–1294, 2007.

[52] S. Sigismund, D. Avanzato, and L. Lanzetti, "Emerging functions of the EGFR in cancer," *Mol. Oncol.*, vol. 12, no. 1, pp. 3–20, 2018, doi: 10.1002/1878-0261.12155.

[53] H. Y. Ng *et al.*, "Chemotherapeutic treatments increase PD-L1 expression in esophageal squamous cell carcinoma through EGFR/ERK activation," *Transl. Oncol.*, vol. 11, no. 6, pp. 1323–1333, 2018, doi: 10.1016/j.tranon.2018.08.005.

[54] L. Fournel *et al.*, "Cisplatin increases PD-L1 expression and optimizes immune check-point blockade in non-small cell lung cancer," *Cancer Lett.*, vol. 464, pp. 5–14, 2019, doi: 10.1016/j.canlet.2019.08.005.

[55] L. Guo *et al.*, "Variation of programmed death ligand 1 expression after Platinum-based neoadjuvant chemotherapy in lung cancer," *J. Immunotherapy*, vol. 42, no. 6, pp. 215–220, Jul./Aug. 2019, doi: 10.1097/CJI.0000000000000275.

[56] B. A. Brakel, C. R. Chokshi, S. K. Salim, C. Venugopal, and S. Singh, "In vitro evaluation of CAR-T cells in patient-derived glioblastoma models," *STAR Protoc.*, vol. 2, no. 4, 2021, Art. no. 100920, doi: 10.1016/j.xpro.2021.100920.

[57] Z. Chen *et al.*, "3D hanging spheroid plate for high-throughput CAR T cell cytotoxicity assay," *J. Nanobiotechnol.*, vol. 20, no. 1, 2022, Art. no. 30, doi: 10.1186/s12951-021-01213-8.

[58] R. Bughda, P. Dimou, R. R. D'Souza, and A. Klampatsa, "Fibroblast activation protein (FAP)-Targeted CAR-T cells: Launching an attack on tumor stroma," *Immunotargets Ther.*, vol. 10, pp. 313–323, 2021, doi: 10.2147/ITT.S291767.